Journal of the Mechanics and Physics of Solids 70 (2014) 227–241

Contents lists available at ScienceDirect

Journal of the Mechanics and Physics of Solids

journal homepage: www.elsevier.com/locate/jmps

A stochastic description on the traction-separation law of an interface with non-covalent bonding

Yujie Wei

LNM, Institute of Mechanics, Chinese Academy of Sciences, Beijing 100190, People's Republic of China

ARTICLE INFO

Article history:
Received 4 August 2013
Received in revised form
27 February 2014
Accepted 27 May 2014
Available online 4 June 2014

Keywords:
Stochastic interface
Cohesive model
Bonding/debonding
Rate-sensitivity
Adhesion

ABSTRACT

We formulate a stochastic description about the mechanical response of an interface composed of non-covalent bonds. In such interfaces, the evolution of bonding probability in response to deformation plays the central role in determining their traction-separation behavior. The model connects atomistic and molecular level bonding properties to meso-scale traction-separation relationship in an interface. In response to quasi-static loading, the traction-separation of a stochastic interface is the resultant of varying bonding probability as a function of separation, and the bonding probability follows the Boltzmann distribution. The quasi-static stochastic interface model is applied to understand the critical force while detaching a sphere from an infinite half space. We further show the kinetics of interfacial debonding in the context of the Bell model (1978) and two of its derivatives – the Evans-Richie model (1997) and the Freund model (2009). While subjected to constant force, an interface creeps and its separation–time curve shows typical characteristics seen during the creep of crystalline materials at high temperature. When we exert constant separation rate to an interface, interfacial traction shows strong rate-sensitivity with higher traction at faster separation rate. The model presented here may supply a guidance to bring the stochastic nature of interfacial debonding into theories on cracking initiation and growth during fatigue fracture.

1. Introduction

Most biological structures and synthetic materials are composed of interfaces, which enable the microstructures to bond coherently to form macroscopic systems. In many circumstances, interfaces are specially tuned to realize particular performance or function of the materials, and their mechanical behaviors are crucial for bottom-up design in hierarchical materials (Hutchinson and Evans, 2000). Understanding the mechanical behavior at the interfacial level is hence crucial for property control in materials, and is the key for further property-structure optimization. At the continuum level, the mechanics of a cohesive interface is assumed to obey a traction-separation constitutive relation–a concept originally proposed by Barenblatt (1959) and Dugdale (1960). Combining with the finite-element procedure, the convenience of cohesive modeling in understanding fracture behavior in materials was recognized by Needleman and others (Needleman, 1990; Xu and Needleman, 1994). By putting cohesive zones in the interfaces in materials, many groups (e.g., Needleman, 1990; Tvergaard and Hutchinson, 1992; Xu and Needleman, 1994; Camacho and Ortiz, 1996; Yang et al., 1999; Gao and Bower, 2004; Wei and Anand, 2004; Su et al., 2004; Warner et al. 2006; Wei et al., 2009) demonstrated the capability to

E-mail address: yujie_wei@lnm.imech.ac.cn

http://dx.doi.org/10.1016/j.jmps.2014.05.014
0022-5096/

track crack initiation, crack propagation, and crack branching etc., which otherwise could only be seen via tedious and expensive experiments. Along this line, different phenomenological interface models have been proposed to represent the physics of different types of bonds across an interface. For example, Xu and Needleman (1994) and Needleman (1990) suggested a potential-based traction-separation law to describe the interfacial fracture, which provides a framework for directly simulating crack branching phenomena. To model the failure of a polycrystalline system subjected to dynamic loading, Camacho and Ortiz (1996) used a cohesive law in which its initial cohesive response is rigid, and there is a critical traction at which strength softening starts. Wei and Anand (2004) later on developed an elastic–plastic interface model which accounts for both reversible elastic, as well as irreversible inelastic separation-sliding deformation at the interface prior to failure. Gurtin and Anand (2008) further formulated a gradient theory of nanocrystalline grain boundaries where displacement discontinuity occurs, via which elastic and inelastic descriptions of slip and separation in grain boundaries were deduced. Regardless of the success and broad usage of those cohesive models, caution should be always exercised as we apply a cohesive model to a particular question. The real mechanics of an interface could be very sensitive to the type of law we choose. For example, Wei and Hutchinson (1997) revealed that under large scale yielding, the notion of a thickness-independent interface toughness no longer pertains, and a nonlinear fracture mechanics is required to quantify interfacial failure. Falk et al. (2001) have found that finite element calculations of dynamic fracture based on embedded cohesive surfaces in a continuum indicate that the predictions are sensitive to the cohesive law used. Cohesive laws that have an initial elastic response were observed to produce spontaneous branching at high velocity. However, crack branching behavior was not observed when cohesive laws that are initially rigid were implemented. The sensitivity of mechanical behavior on the exact form of cohesive laws hence calls for more physically sound understanding about the cohesive behavior of interfaces. One effective way is to bridge the traction-separation law of an interface with the atomistic origin of bonds in the interface. The cohesive model using the virtual-internal-bond concept is one example to build up a linkage between atomistic interaction to continuum models (Gao and Klein, 1998a; 1998b). Jiang et al. (2006) developed more specific cohesive laws for particular interfaces bonding via the van der Waals interaction. Warner et al. (2006) have calibrated cohesive laws by abstracting parameters from atomistic level simulations using empirical potentials. Experimental methods are also suggested to probe the interface cohesive laws in particular system (e.g., Hong et al., 2009).

It is worth noting that those phenomenological continuum models and atomistic-mechanism based models are essentially for one way transition from bonding state to rupture. At the atomistic scale, in particular for an interface composed of non-covalent bonds, molecular bonds at an interface undergo concurrent bonding and debonding while subjected to external disturbance, and may reach its equilibrium at a given state only if we wait sufficiently long. The scenario might be the exact cases in biological systems, where connections between different structures are typically achieved via non-covalent bonding, and their mechanics is associated with chemi-mechanical transduction (Tidball, 2005). Such bonding and debonding kinetics could give rise to rich biological phenomena, and is of significance for the activities of cell, such as cell adhesion and cell mobility (Thomas et al., 2002; Marshall et al., 2003, Phan et al., 2006; Lin and Freund, 2007, Lin et al., 2008; Wei, 2008a, 2008b) and the life time of bonds. There is emerging effort to develop understanding about the mechanics of stochastically bonded interfaces in biological systems. For example, Deshpande et al. (2006, 2008) applied the cohesive model concept to develop a bio-mechanical model while coupling cell contractility with focal adhesion formation. Qian et al., (2008, 2009) and Wang and Gao (2008) performed simulations and developed theoretical models about the lifetime and the strength of periodic bond clusters between elastic media. With the growing evidence that cells may not only sense the mechanical properties of substrates (e.g., Lo et al., 2000; Engler et al., 2006) but also respond actively to external dynamic loading (e.g., Jungbauer et al., 2008), there is compelling need to develop atomistic dynamics based cohesive interface composed of non-covalent bonds for such systems as well, in order to build connections between atomistic and molecular level bonding properties and meso-scale measurable quantities.

In this paper, we describe a model that suggests that the traction-separation at an interface composed of non-covalent bonds is governed by stochastic bonding-debonding process, and develop stochastic-based traction-separation laws capable of connecting atomistic/molecular level interface properties to meso-scale description. At quasi-static loading, it is thought that at a given separation, the bonding probability follows the Boltzmann distribution. Dynamic response of an interface is regarded as debonding ascribed by the diffusive process. This process resembles chemical potential driven vacancy nucleation and diffusion in crystalline solids. In the following sections, we first describe the stochastic cohesive model in an interface composed of non-covalent bonds, with the static case discussed first and followed by the dynamic response of a stochastic interface. At the end, we apply the stochastic traction-separation model to the bench mark problem of finding the critical detachment and the stability of adhesion when one body is in contact with an elastic half space.

2. Traction-separation law governed by stochastic bond dissociation

We consider a bond complex as illustrated in Fig. 1. The spring-bond system may represent actual mechanical behavior of fundamental units in natural and artificial composite structures where interfaces are bonded via polymer chains (e.g., Smith et al., 1999; Wiita et al., 2007), such as DNA unfolding while being stretched, the response of force spectroscopy (e.g., atomic force microscopy) while measuring adhesion or friction properties of surfaces (e.g., Binnig et al., 1986; Marshall et al., 2003), the hairy attachment from the lowest hierarchical spatula in gecko by van deer Waals interaction (Autumn et al., 2002; Huber et al., 2005), and so on. The bond itself is depicted by the potential energy $U(r)$ at its reaction coordinate r. The structure in Fig. 1 is best for interactions which could be approximated by pair potentials. The chain is described by

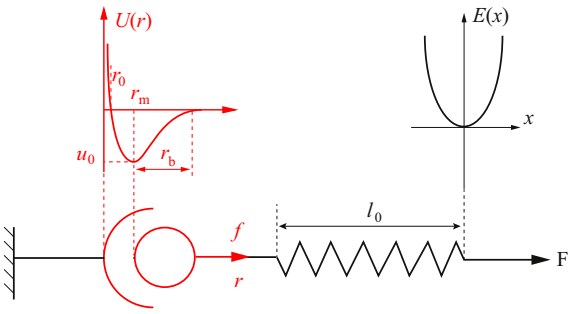

Fig. 1. Illustration to show the two parts of a bond complex, the bond pocket characterized by a potential function $U(r)$ and the spring system. Bond rupture is controlled by the modified potential due to the change in r when force/displacement is applied to the complex.

a free energy $E(x,t)$ at the stretching distance x while the complex is subjected to tensile loading F at the time t. The transmitted force will change bond energy and reaction coordinate r, and the latter is also connected with x. Hence $U(r)=U(r(x))$. We are interested in developing the traction-separation law for a cohesive interface composed of such potential bonding sites of density $\rho(z)$ (per unit area at the position z). Note that there may exist a difference between the load F to the chain and the load f acting directly along the reaction coordinate, in particular for bonded DNAs or polymer chains in viscous media. At this moment, we neglect this effect and we assume what transmitted to the bond is force but not displacement. A representative surface is assumed to compose of sufficiently large number of bonds so that it is statistically meaningful to derive the collective response of those bonding sites.

At the separation distance x and at the time t, we define a bonding probability function $b(x,t)$, which refers to the fraction of closed bonds in a unit surface with bonding site density $\rho(z)$. A generic form of traction $T(x,t;z)$ (force per unit area) can then be deduced

$$T(x,t;z)=\rho(z)b(x,t)\frac{\partial E(x,t)}{\partial x} \tag{1}$$

In what follows, we will use a constant distribution of bond density ρ. To connect Eq. (1) with commonly known traction-separation laws, we consider an interface with all bond complexes being either closed or ruptured. A closed bond has a lower energy level in contrast to a ruptured bond by an amount of u_0. At equilibrium and when no traction is exerted to the interface, $b(x,t)$ is independent of the time t and follows a Boltzmann distribution:

$$b(x,t)=b_0=\frac{1}{1+\exp(-u_0/k_BT)}=\frac{1}{1+\exp(-\beta u_0)} \text{ with } \beta=\frac{1}{k_BT}, \tag{2}$$

where k_B is the Boltzmann constant and T is the absolute temperature. If the interface is forced to separate under external loading, i.e., the right hand side of bond complex in Fig. 1 has the displacement x, which consequently modifies the potential landscape of the bond on the left hand side. The energy barrier u_0 is lowered to be $U(r(x))$. It is noted that we apply quasi-static displacement controlled loading at this moment in order to derive the general form of traction-separation law for a non-covalent bond interface. Now the ratio of closed bonds will be altered to be

$$b(x)=\frac{1}{1+\exp[-\beta U(r(x))]}. \tag{3}$$

Following Eq. (1), we obtain the induced traction at the prescribed separation x:

$$T(x)=\frac{\rho}{1+\exp[-\beta U(r(x))]}\frac{\partial E(x)}{\partial x}=\frac{\rho}{1+\exp[-\beta U(r(x))]}\frac{\partial U(r)}{\partial r}. \tag{4}$$

In the above equation, we have used the force equilibrium condition in the bond complex at static state,

$$\frac{\partial U(r)}{\partial r}=\frac{\partial E(x)}{\partial x}. \tag{5}$$

With known $U(r)$ and $E(x)$, we can proceed to obtain the time-independent traction-separation law based on stochastic bonding process at an interface. For simplicity but without loss in physics, we may use simple forms for both $U(r)$ and $E(x)$.. We first consider the potential model proposed by Bell (1978). An applied force may modify the potential of the bond pocket following

$$U(r)=u_0-f\,r_b, \tag{6}$$

where f is force transmitted to the bond in response to the separation x and r_b is the characteristic width of the potential well. A detailed illustration of the energy landscape is given in Fig. 2.

Typically, for van der Waals bonds in biological systems, r_b is on the order of nanometers (Evans and Ritchie, 1997). Let $E(x)=k_cx^2/2$ where k_c is the stiffness of the chain (note that more complicated spring behavior could be used here).

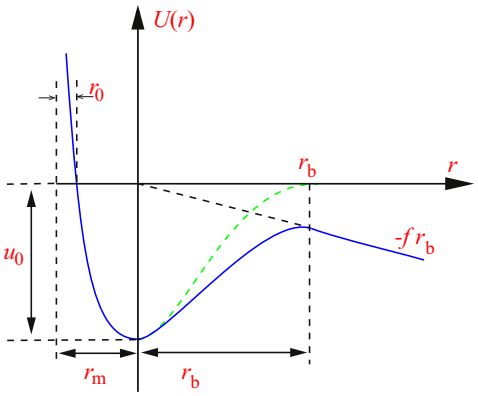

Fig. 2. Demonstration to show how the energy landscape $U(r)$ in the Bell's model is tilted by external load. The parameters of the potential well are shown, with r_0 being the zero energy distance, and r_m is where the energy reaches its minimum of u_0.

Table 1
Three groups of bond properties used for Eq. (7), which give rise to corresponding time-independent traction-separation response shown in Fig. 3a–c.

Type	k_c (N/m)	$u_0(kT)$	r_b(Å)
Flexible	0.2	4	5
Intermediate	1.0	40	4
Stiff	10	400	3

By applying $f=\partial E(x)/\partial x$ and substituting Eq. (6) into Eq. (4), we obtain the time-independent traction-separation law as

$$T(x)=\frac{\rho\, k_c x}{1+\exp[\beta(-u_0+f\, r_b)]}=\frac{\rho\, k_c x}{1+\exp[\beta(-u_0+k_c x\, r_b)]} \tag{7}$$

We explore the traction-separation governed by stochastic bonding in an interface using Eq. (7). In Table 1, we listed the bond energy, bond stiffness and potential well width for several typical bonds. Fig. 3a–c shows respectively, the traction-separation curves of flexible, intermediate, and stiff interfaces. Here we have used a bond density of $\rho=10^{19}$ bonds/m^2, which is about 10 bonds in one square nanometer and is close to the number of nearest neighbor bonds between two atomic planes in crystalline materials. The density in most interfaces could be actually lower than this number. While the flexible interface shows rather slow drop in traction after the peak (Fig. 3a), tractions decrease progressively with strain after the strength peak in a stiff interface (Fig. 3c). It resembles a gradual failure to abrupt rupture transition as we increase the stiffness of an interface.

The actual potential of the bond pocket could be more complex. For example, the 6–12 Lenard-Jones potential is broadly used to represent the van der Waals interaction between biological bonds, which the potential function is given as

$$U(r)=4u_0\left[\left(\frac{r_0}{r}\right)^{12}-\left(\frac{r_0}{r}\right)^{6}\right],\ \text{at } r_m=\sqrt[6]{2}\, r_0=1.123r_0,\ \ U_m=-u_0. \tag{8}$$

An explicit expression for traction-separation laws is not available in that case. We may numerically solve the traction-separation relation via the following steps:

(a) For an applied displacement X to the bond complex, it contains two contributions, the position change $r-r_m$ by the bond (assuming the bond is at the lowest energy point r_m at the beginning), and the displacement in the chain x, i.e., $X=x+(r-r_m)$;
(b) Applying force equilibrium in Eq. (5), we have $-(24u_0/r_0)\,[2(r_0/r)^{13}-(r_0/r)^7]=k_c[X-(r-r_m)]$;
(c) In the case of extremely stiff chains, i.e., $k_c\to\infty$, we may either replace the right hand side by f when force controlled boundary is applied, or r is known when displacement controlled boundary is exerted;
(d) Solving the above equation for r, we can subsequently derive x, f, and $U(r)$, and then the bonding probability by substituting $U(r)$ in Eq. (3);
(e) With known bonding probability at each separation X, we obtain the traction-separation law using Eq. (4). When the stiffness of the chain is rather small, i.e., $r-r_m\ll x$, we may simply use x as the separation of the bond complex instead of X.

In Fig. 4, we show an example of traction-separation laws in interfaces governed by LJ interaction. The influence of chain stiffness k_c on the traction-separation law are demonstrated. In Fig. 4a, several traction-separation curves using

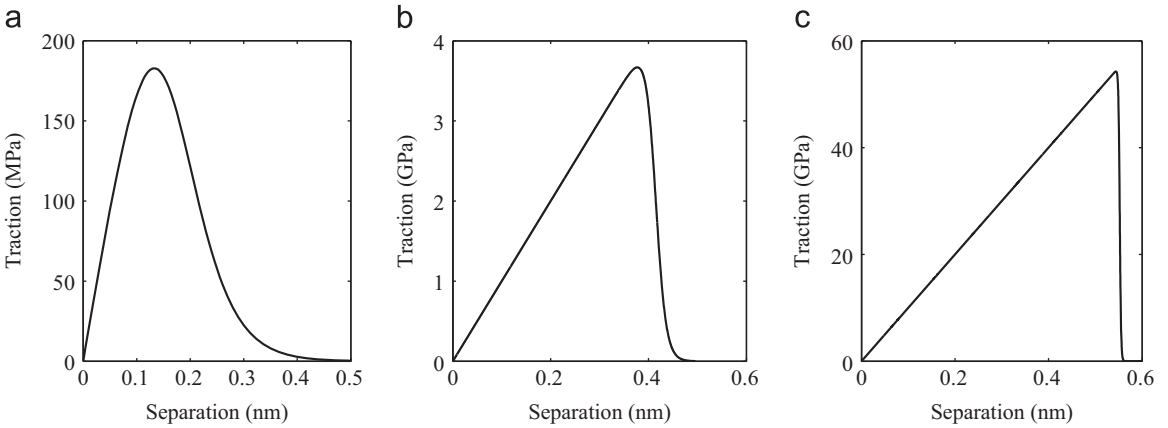

Fig. 3. The static traction-separation governed by stochastic bond rupture in an interface given by Eq. (7). (a) Traction-separation for a flexible interface. (b) Traction-separation for an intermediate interface. (c) Traction-separation for an extremely stiff interface.

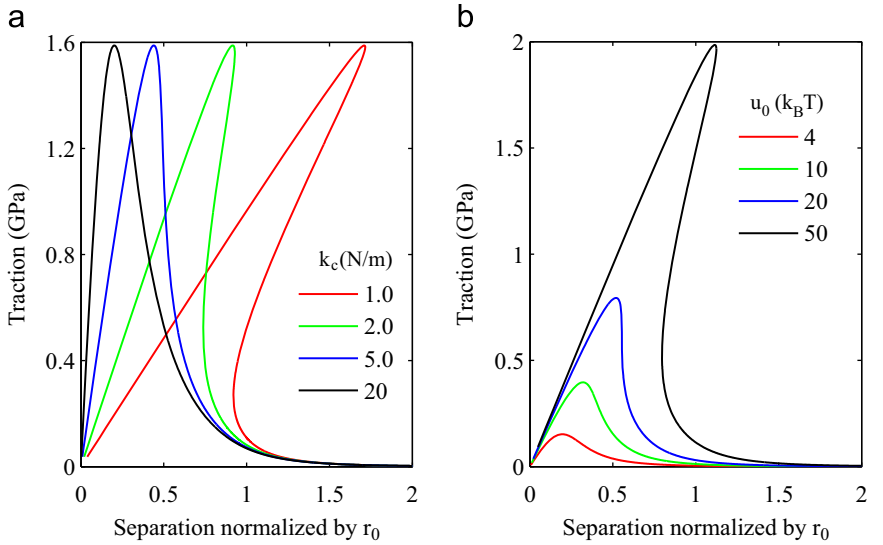

Fig. 4. Corresponding traction-separation behavior in an interface governed by the LJ bonding. (a) Traction-separation for bonds with four different chain stiffness k_c in unit of N/m. Here $r_b = 5 \times 10^{-10}$ m and bond energy $u_0 = 40k_BT$. (b) Traction-separation for bonds with four different bond energy u_0 in unit of k_BT ($k_c = 2$ N/m and $r_b = 5 \times 10^{-10}$ m). We note that lower stiffness in the chain and higher bond energy of the bond pocket tend to induce separation instability.

$r_b = 5 \times 10^{-10}$m and $u_0 = 40kT$ in the LJ potential in Eq. (8) are presented. We see that lower stiffness k_c in the chain may induce separation instability: After the peak traction, the interfacial separation, which is the combination of bond separation and the chain elongation, could actually bounce back due to the traction-softening, and the latter results in more deformation relaxation in the chain than the extension in the bond pocket. It is noted that this phenomenon is due to the condition that we allow the bond separation r to increase monotonically. This instability makes the interface brittle like. High bond energy for the bond pocket will give rise to the same type of separation instability as demonstrated in Fig. 4b, where we have used a chain stiffness of $k_c = 2N/m$ and a bond potential well width of $r_b = 5 \times 10^{-10}$m.

In both Eqs. (4) and (7), the traction maximizes at the separation x_m satisfies $\partial T(x)/\partial x = 0$. Taking Eq. (7) as the example, the maximum traction can be obtained by solving the following equation for x_m:

$$(\beta k_c x_m r_b - 1)\exp[\beta(-u_0 + k_c x_m r_b)] - 1 = 0. \tag{9}$$

With x_m from Eq. (9), we obtain the maximum traction:

$$T_m = \rho\left(k_c x_m - \frac{k_B T}{r_b}\right). \tag{10}$$

The asymptotic solution to Eq. (9) is

$$x_m = \frac{u_0}{k_c r_b} - \frac{\ln \beta u_0}{\beta k_c r_b}, \tag{11}$$

and corresponding asymptotic formulation for the maximum traction is

$$T_m = \frac{\rho}{r_b}\left[u_0 - k_B T(\ln \beta u_0 + 1)\right]. \tag{12}$$

As shown in Fig. 5, the asymptotic solution is very close to the numerical solution as $u_0 \geq 12 k_B T$, where the relative difference is within 1%. We find that at equilibrium the maximum traction is independent of the chain stiffness k_c.

It is also convenient to derive the surface energy of two materials in contact. Let γ_a and γ_b the surface energies of the two materials, respectively, and γ_{ab} be the interfacial energy of the two materials in contact. For an ideally flat surface, the adhesion energy Γ of the two surfaces will lead to

$$\Gamma = \gamma_a + \gamma_b - \gamma_{ab} = \rho b(x=0) u_0 = \frac{\rho u_0}{1+\exp(-\beta u_0)}, \tag{13}$$

Eq. (13) essentially builds up a connection between the atomistic level bonding information in an interface with its macroscopically measurable interfacial energy. We will further show that the stochastic bonding controlled interfacial model can be applied to describe the adhesion of a sphere (or a infinitely long cylinder) in contact with an infinite half space elastic medium in Section 4.

We may further build up a connection between the atomistic bond information with the fracture toughness G_0 for the traction-separation law given in Eq. (7). The energy to separate the interface from the traction-free bonding state to infinite distance is given as

$$G_0 = \int_0^\infty T(x)\, dx = \frac{\rho\, k_c}{(\beta k_c\, r_b)^2} \int_0^\infty \frac{t}{1+\exp(t-u)} dt \quad \text{with} \quad u = \beta u_0 \tag{14}$$

The integral at the right hand side of Eq. (14) is one of the integrals of the Fermi–Dirac distribution (Weisstein, 2014), which has a closed form expression

$$\int_0^\infty \frac{t^s}{1+\exp(t-u)}\, dt = -\Gamma(s+1)\mathrm{Li}_{1+s}(-e^u) \ \text{ for } \ s \geq -1 \tag{15}$$

where Γ is the Gamma function and $\mathrm{Li}_{1+s}(-e^u)$is the Polylogarithm function. With Eqs. (14) and (15), we now obtain the close form expression of fracture toughness

$$G_0 = -\frac{2\rho\, k_c}{(\beta k_c\, r_b)^2}\mathrm{Li}_2(-e^{\beta u_0}), \ \text{ and } \ G_0 \approx u_0 k_B T \frac{\rho\, k_c}{(k_c\, r_b)^2} \ \text{ when } \ \beta u_0 \gg 1. \tag{16}$$

We have used the limitation of

$$\lim_{\mathrm{Re}(u)\to\infty} \mathrm{Li}_{1+s}(-e^u) \ = -\frac{u^s}{\Gamma(s+1)} \tag{17}$$

in the last step of Eq. (16). Note that the close form expression of fracture toughness may be only available for simple potential models like the Bell model (Bell, 1978). We have to rely on numerical methods in more sophisticated potentials.

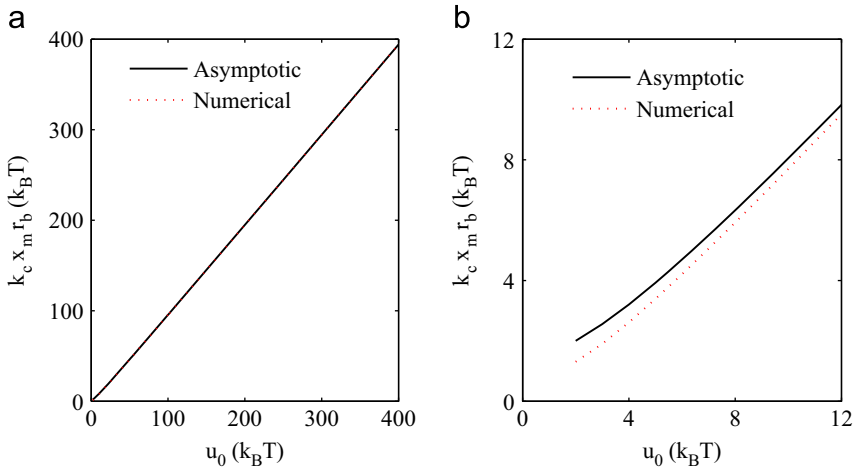

Fig. 5. Comparison of the asymptotic solution and numerical results for the location where the traction maximizes. (a) The asymptotic expression matches well with the numerical solution in a wide range of the energy of the potential well. (b) Amplification to show the difference when the energy is low.

With the current development of the interfacial model, we are already able to bring in experiments from the literature for some simple validations. We consider graphene and graphite, which seem to be one of the most mechanically characterized materials at both atomistic scale and macroscopic scale in recent years. Experimental measurement for cleavage energy along the c-axis in graphite is about 61 ± 5 meV/atom (Zacharia et al., 2004), that would give the van der Waals potential energy between C-C bonds to be about $u_0=61\pm5$ meV/atom. With Eq. (13), we obtain an adhesive energy to be 0.34 J/m^2. This number is in good agreement with recent measurement of 0.31 J/m^2 for the adhesive energy of multi-layer graphene (Koenig et al., 2011). In addition, by taking $r_b=0.34$ nm (which is the interlayer distance in graphite), we predict with Eq. (12) that the peak strength to separate graphite along its c-axis is about 230 MPa. As the van der Waals potential energy between C–C bonds is close to the thermal energy k_BT at room temperature (about 0.026 meV/atom), the predicted peak strength is very sensitive to u_0. For example, when $u_0=40$ meV/atom, the predicted peak strength drops to 51 MPa. That may explain why current measurement for the cleavage strength of graphite show huge scattering.

3. Dynamical response of a stochastic interface

In the previous section, we formulated the mechanical behavior of an interface governed by stochastic when bonding-rupture events are an extremely slow process and the mechanical behavior is regarded to be quasi-static. In many real applications, time and deformation rate are indispensable to understand interfacial failure. A significant difference between the static response and the dynamics behavior in an interface is the high rate sensitivity of traction predicted by dynamic models. Existing theories about the kinetic debonding are built upon the one-dimensional Kramers' reaction rate theory (Kramers, 1940), and have been applied successfully in molecular level mechanics (Zhurkov, 1965; Bell, 1978; Evans and Ritchie, 1997; Freund, 2009). In this scheme, it is assumed that debonding occurs diffusively rather than ballistically (Freund, 2009) along its reaction coordinate. The probability function k_{off}, also called the off-rate, quantifies the transition chance of a closed bond to become ruptured in a unit time, and is the key parameter for bond kinetics. A simple yet very successful model for the bond off-rate was suggested by Bell (1978)

$$k_{off}=\upsilon_0\exp(-\beta u_0)\exp(\beta f\, r_b). \tag{18}$$

where υ_0 is a constant rate characterized by bond vibration. To fully utilize the successful debonding theories for single molecules (Bell, 1978; Evans and Richie, 1997; Freund, 2009) and bridge the atomistic level bond properties to meso-scale interfacial mechanics, we further extend the dynamic debonding model for single molecules by (a) considering both bond rupture and rebonding mechanisms which could be of significance for biological systems like cell motion, and by (b) describing the evolution of the density of closed bonds in an interface, rather than the instantaneous rupture of all closed bonds, in order to capture the gradual degradation and failure process occurring at an interface.

3.1. Evolution of bond density in an interface

We depart from the models for a single bond complex, and assume that debonding is a thermally activated process driven by the change in free energy per unit area resulting from an increase in load. We define an excessive free energy of a representative unit surface by taking (Wei et al., 2010)

$$\Delta\mu=\rho\, k_BT\log[b(x,t)/b_e]+\delta U(x,t), \tag{19}$$

where b_e is the equilibrium bond concentration in a unit area at a prescribed separation x. The first term in Eq. (19) represents an entropic contribution to the free energy change; while the second is the work done by external load. At a given separation x, the bond density at infinite time t follows the Boltzmann distribution and is given in Eq. (3)

$$b(x,t\to\infty)=b_e(x)=\frac{1}{1+\exp[-\beta U(r(x))]} \tag{20}$$

Here $U(r(x)=-u_0+\delta U(x,t)$. The rate of debonding is assumed to follow as

$$\rho\frac{\partial\, b(x,t)}{\partial\, t}=-\frac{k_{off}}{k_BT}\Delta\mu=-\beta\, k_{off}\Delta\mu, \tag{21}$$

where k_{off} is assumed to be a constant, and a more complicated case can be considered. It is further noted that in Eq. (21), we neglect possible threshold strength for bond breakage. This mechanism could certainly be included to model richer interfacial behavior, in particular when debonding is more ballistic like rather than diffusive like.

Now we proceed to derive $b(x,t)$ once the reaction coordinate and the initial conditions are given. While the idea can be applied to any boundary condition, we particularly show the dynamical interfacial behavior for two special cases: an interface subjected to constant force or under a constant separation rate.

3.2. Force controlled interfacial creeping

We first consider the case of force loading and assume we know the force at any given time. In this circumstance, we set the clock to time $t=0$ as the step load F acts directly on a unit area. We hence have $\delta U(x,t)=F\,x$. We define a macroscopic

interfacial stiffness K_m which connects with the stiffness of individual bonds via $K_m = \rho b(x,t) K_b$. Here K_b is a lumped stiffness which is slightly different from k_c and K_b includes the contribution from both the chain and the bond pocket. In most polymeric bonding, we expect $K_b \approx k_c$. Force equilibrium at any instance requires $F = K_m\, x = \rho b(x,t) K_b\, x$. We set the initial bond density (right before the load F being applied) to be $b(x, t=0) = b_0$. The applied load will give rise to a separation jump $x_0 = F/\rho b_0 K_b$. At any other time, the separation x is a resultant of F, and can be determined via the force equilibrium condition as

$$x = \frac{F}{\rho b(x,t) K_b} \tag{22}$$

Now with Eq. (21), we have the evolution of bond density in terms of the applied force:

$$\frac{\partial\, b(x,t)}{\partial\, t} + k_{off}\, \log\left[\frac{b(x,t)}{b_e(x)}\right] = -\beta\, k_{off} \frac{F^2}{\rho^2 b(x,t) K_b}. \tag{23}$$

We may develop some elementary understanding on Eq. (23) by neglecting the second term on the left hand side. It is convenient to obtain

$$b^2(x,t) = b_0^2 - 2\beta\, k_{off} \frac{F^2}{\rho^2 K_b} t \tag{24}$$

In Eqs. (23) and (24), we have two characteristic time scales t_s and $t_{\max}$, with

$$t_s = 1/\, k_{off} \text{ and } t_{\max} = \frac{b_0^2}{2\beta\, k_{off}} \frac{\rho^2 K_b}{F^2}, \tag{25}$$

and the latter defines the surviving time of the interface. With Eqs. (22) and (24), we now deduce the accumulated separation at the interface as a function of time:

$$x - x_0 = \frac{F}{\rho K_b b_0}\left[\left(1 - \frac{t}{t_{\max}}\right)^{-1/2} - 1\right]. \tag{26}$$

We show in Fig. 6 the evolution of separation as a function of time given in Eq. (26). It is noted that the incremental separation shows three characteristic stages resembling the creep to rupture behavior of materials at high temperature: the primary stage with fast growth rate, the secondary stage with nearly steady state growth rate of separation, as well as the tertiary stage where the interface separation accelerates quickly to its final point where the interface losses its capability for load carrying.

Now we resort to numerical methods to understand the influence of the second term on the right hand side of Eq. (23) on the mechanics of a stochastic interface. For simplicity, we use the dimensionless form of the equation by letting $\tilde{t} = k_{off}\, t$, $\tilde{x} = (x/x_0) = (x\rho b_0 K_b/F)$, $\tilde{b} = (b(x,t)/b_0)$, with which we have

$$\frac{\partial\, \tilde{b}(\tilde{x},\, \tilde{t})}{\partial\, \tilde{t}} = -\frac{1}{b_0} \log\left[\frac{b_0 \tilde{b}(\tilde{x},\, \tilde{t})}{b_e(\tilde{x})}\right] - \frac{\zeta}{b_0 \tilde{b}(\tilde{x},\, \tilde{t})}, \text{ with } \zeta = \frac{\beta F^2}{\rho^2 b_0 K_b} \tag{27}$$

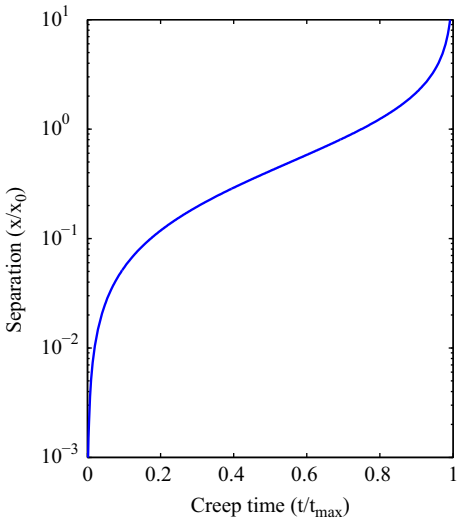

Fig. 6. Interfacial separation as a function of creep time, which shows different stages of separation increase. It resembles the creeping behavior of materials at high temperature.

From Eq. (27), we see that it is possible for the right hand side to be zero, indicating that the entropic driven rebonding is capable of matching the debonding at an applied force. It hence suggests that the interface will have a theoretically infinite life-time under the applied load. In other circumstances, the interface will have a finite life-time. Given the diversity of interfacial bonds, the dimensionless bond dissociation rate ζ could vary largely. In Table 2, we show typical parameters which are close to many real adhesively jointed interfaces. This group of materials/interfacial parameters gives rise to a dissociation rate close to k_{off}, and supplies guidance in case the readers wants to use the model in their own systems, combining Eqs. (20), (22) and (27) to solve the evolution of bond density and interface separation. In Fig. 7a, we show the evolution of bonding probability as a function of time for different dimensionless bond dissociation rate ζ.

With Eqs. (20) and (27), we can then deduce the creeping history of the interface under constant force, and this information is given in the separation-time curves in Fig. 7b for several different ζ. So far, we have discussed the dynamic behavior of an interface subjected to constant load, next we will consider the situation when displacement controlled loading is applied.

3.3. Displacement controlled interface separation

While the model discussed here can essentially be applied to arbitrary displacement-controlled loading history, we focus on the case of constant separation rate. With $dx/dt = V$, we can now rewrite Eq. (23) as

$$\frac{\partial b(x,t)}{\partial t} + k_{off}\log\left(\frac{b(x,t)}{b_e(x)}\right) = -\beta\, k_{off} b(x,t) K_b (Vt)^2. \tag{28}$$

Table 2
Typical parameters for an adhesively joint interface, with which we obtain the dimensionless bond dissociation rate ζ.

Parameters	Value	Explanation
E	10 GPa	Interfacial modulus
k_B	1.38×10^{-23} J/K	The Boltzmann constant
T	300 K	Room temperature
β	2.5×10^{20} J^{-1}	$\beta = 1/k_BT$
u_0	$10k_BT$	Bond energy
b_0	≈ 1 (using Eq. 2)	Initial bonding probability
ρ	10^{18} bonds/m^2 (1/nm^2)	Bond surface density
F	2×10^{7} N	Applied force (per m^2)
F/ρ	2×10^{-11} N (20 pN)	Average force per bond
σ	20 MPa	Interfacial stress
K_b	100 pN/nm	Bond stiffness
x_0	2×10^{-11} m (2 Å)	Initial separation by F
ζ	1.0	Dimensionless bond dissociation rate

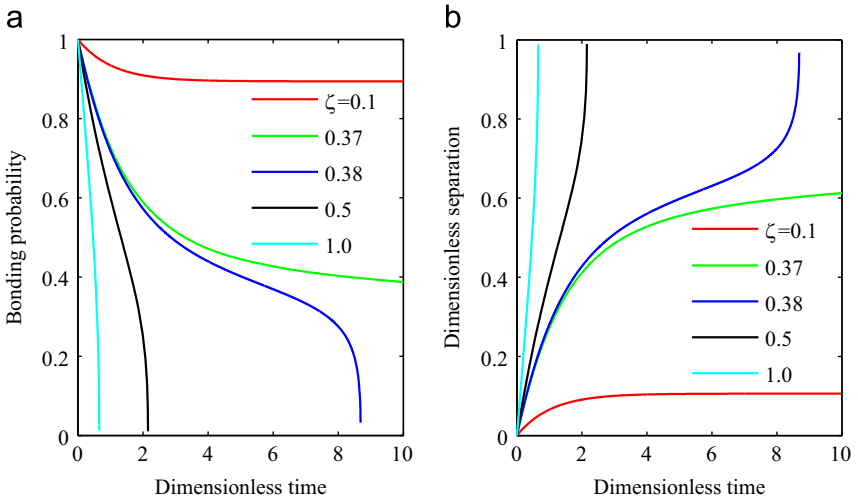

Fig. 7. (a) Bonding probability as a function of time described by Eq. (38). Here several different ζ is explored to show the critical value: above which the interface will have an infinite life time under the applied load; blow that the interface will have a finite lifetime. This transition is associated with a critical force following Eq. (27). (b) Interfacial creep under constant loading.

Similar to the discussions on constant loading, we first consider the case where debonding dominates and entropy driven recovery is negligible. In this circumstance, we drop the second term on the left-hand side of Eq. (28) and obtain

$$b(x,t) = b_0 \exp\left(-\frac{\beta\, k_{off} K_b}{3\, V} x^3\right), \tag{29}$$

Now the traction-separation behavior is

$$T(x,t) = \rho b_0 K_b\, x \exp\left(-\frac{\beta\, k_{off} K_b}{3\, V} x^3\right). \tag{30}$$

We show in Fig. 8a the traction–time curves, where the maximum traction increases at higher loading rates. Typical traction-separation curves at higher separation rates are given in Fig. 8b. The maximum traction can be obtained from Eq. (30) as

$$T_{\max} = \rho b_0 K_b\, (3\alpha e)^{-1/3} \text{ at } x = (3\alpha)^{-1/3}, \text{and } \alpha = \frac{\beta\, k_{off} K_b}{3V}. \tag{31}$$

The interfacial toughness, the energy required to separate the interface, can be deduced by

$$G = \int_0^\infty T(x,t)\, dx = \rho b_0 K_b \frac{\Gamma(2/3)}{3}\left(\frac{V}{\xi}\right)^{2/3} \text{ with } \xi = \frac{\beta\, k_{off} K_b}{3}, \tag{32}$$

where we see strong rate sensitivity of released energy as we separate the interface at higher rates, with more energy required at faster separation rate. Now we explore the solution of Eq. (28) by the numerical method. Let $\tilde{b} = (b(x,t)/b_0)$, $\tilde{t} = k_{off}\, t$, and $\tilde{x} = (x/x_0) = (x\rho b_0 K_b/F)$, we have the dimensionless form of the above equation:

$$\frac{\partial\, \tilde{b}(\tilde{x},\tilde{t})}{\partial\, \tilde{t}} = -\frac{1}{b_0}\log\left[\frac{b_0 \tilde{b}(\tilde{x},\tilde{t})}{b_e(\tilde{x})}\right] - \tilde{b}\, \tilde{t}^2 \vartheta, \text{with} \vartheta = \beta K_b \frac{V^2}{{k_{off}}^2}. \tag{33}$$

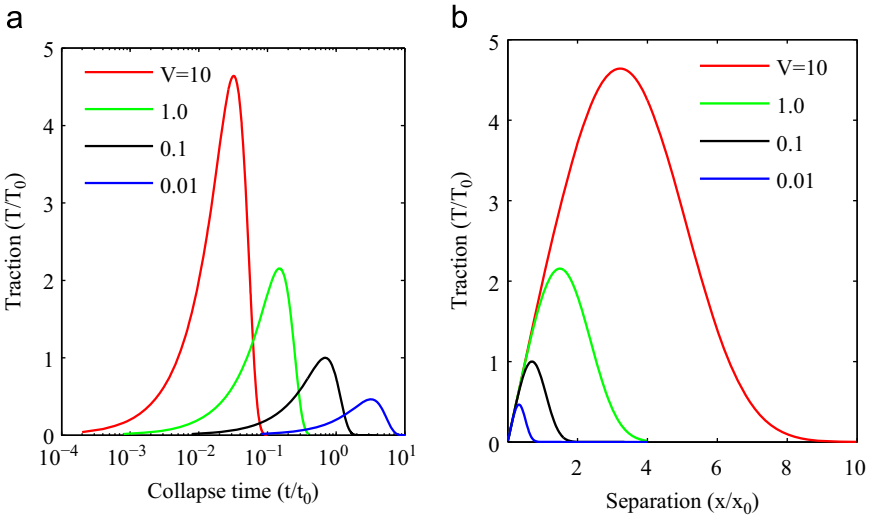

Fig. 8. Dynamics response of a cohesive interface at different separating velocity V in unit of nm/ns. (a) Traction-collapse time curves to show the maximum traction varies with loading rates. (b) Traction-separation. Note that while the life time of an interface decreases at higher separation rates, the separation distance at the point when traction becomes zero becomes greater at higher separation velocity.

Table 3
Typical parameters for an adhesively joint interface subjected to constant separating velocity. Parameters shown here, combined with those listed in Table 1, will lead to a dimensionless debonding rate ϑ on the order of 1.

Parameters	Value	Explanation
k_{off}	1/s	Rate coefficient
V	2×10^{-10} m/s (0.2 nm/ns)	Separating velocity
ϑ	$\sim$1	Dimensionless debonding rate

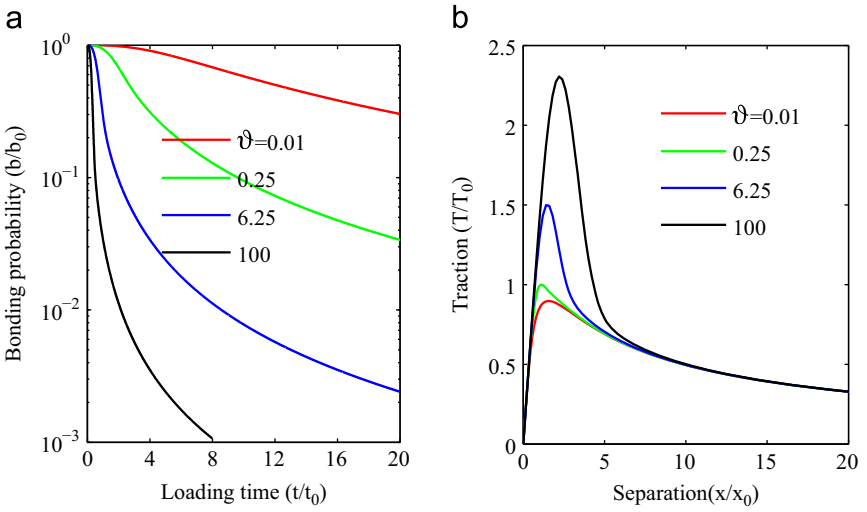

Fig. 9. Dynamics response of a cohesive interface at four different debonding rate ϑ. (a) Bonding probability as a function of time. (b) Traction-separation curves at different separation velocities.

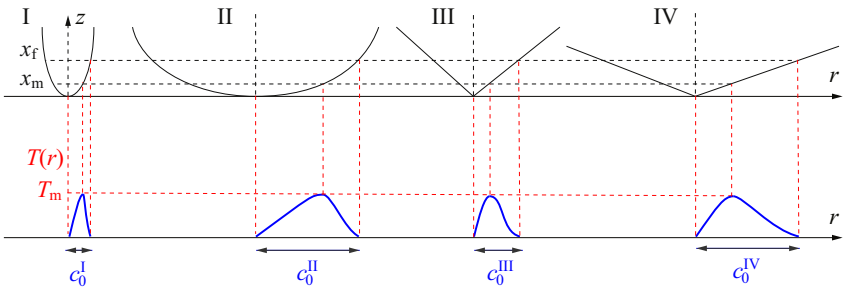

Fig. 10. Illustrations to show that the dependence of adhesion on the detailed geometry of the surface in contact. Although the critical separation x_m where traction maximizes ($T(r)=T_m$) and the maximum allowable separation x_f are fixed, the traction profile $T(r)$ could differ substantially (see the four illustrations above) as a resultant from the difference in the profile of the contacting surface. The actually critical force for detachment is then very sensitive to the shape of the contact zone.

In addition to the parameters listed in Table 3, we also give representative values for the parameters in Eq. (33). The choice of k_{off} and the typical velocity shown in Table 2 will lead to ϑ on the order of 1. In following discussions, the variation of ϑ is solely due to change to the separating velocity V. In contrast to the mechanical behavior of an interface under displacement controlled separation (as shown in Fig. 8), the mechanical response of an interface subjected to constant separation rate shows distinct characteristics when debonding and entropy driven recovery are considered. Fig. 9a shows the evolution of bonding probability as a function of loading time (equivalent to separation as we apply constant velocity). Slow loading rates give rise to gradual decrease in bonding probability. Higher loading rates also result in higher overshoot of the peak traction, and the traction then decreases quickly with separation, as seen in Fig. 9b.

4. Application: detachment of a sphere from an elastic half space.

With above descriptions of traction-separation laws of an interface with non-covalent bonding, we now apply the model to the detachment of a sphere from an elastic half space, which have elastic modulus and Poisson's ratio of (E_1,ν_1) and (E_2,ν_2), respectively. The same type of problem, but in the context of a constant surface adhesion energy, has been considered by Johnson et al., (1971) and Derjaguin et al. (1975; 1983). A more complex surface profile has also been investigated (Guduru, 2007). Here we consider the tensile traction in the contacting zone governed by stochastic bonding. We note that the shape of the traction, and hence the detachment load, is sensitive to the detailed geometry of the profile in contact, as apparently seen in Fig. 10. We assume the surfaces are ideally smooth. The sphere has radius R and interacts with the substrate via non-covalent bonding. In Fig. 11, we show the interfacial stress distribution of a sphere (or a cylinder) adhering to a flat substrate at self-equilibrium. The stress distribution in the compressive zone $P(r)$ is obtained by applying

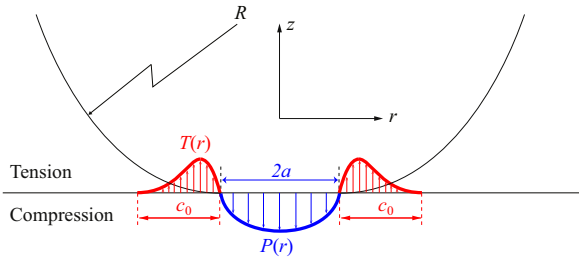

Fig. 11. Illustration to show the interfacial stress distribution of a sphere (or a cylinder) adhering to a flat substrate at self-equilibrium. Here the stress distribution in the compressive zone $P(r)$ is given by the Hertz theory of elastic contact and the tensile cohesive zone has stress $T(r;\delta_z)$ (at position r where the separation between the two bodies in contact is δ_z) governed by the stochastic traction-separation law given in Eq. (4).

the Hertz contact theory between the sphere and the substrate (Hertz, 1896; Johnson 1985), with

$$P(r)=P_0\left[1-\left(\frac{r}{a}\right)^2\right]^{1/2},\quad a=\left(\frac{3F_RR}{4E^*}\right)^{1/3},\quad P_0=\frac{3F_R}{2\pi a^2}=\left(\frac{6F_R(E^*)^2}{\pi^3R^2}\right)^{1/3}\text{ and }\quad \frac{1}{E^*}=\frac{1-\nu_1{}^2}{E_1}+\frac{1-\nu_2{}^2}{E_2},\tag{34}$$

where F_R is the applied force, a is the resultant radius of the contact zone, and E^* is the compound modulus.

At self-equilibrium, F_R is the resultant force from the tensile traction at the peripheral of the contact zone, and is given as

$$F_R=-F_{\text{coh}}=-\int_a^{a+c_0}T(r;\delta_z)\,2\pi r dr,\tag{35}$$

where c_0 is the width of the cohesive zone and F_{coh} is the integral force by adhesion. The tensile cohesive zone has stress $T(r;\delta_z)$ governed by the general stochastic traction-separation law in Eq. (4). Next we aim to derive the pulling force F as we move the sphere away from the surface. The balance of the force requires

$$F+F_R-F_{\text{coh}}=0.\tag{36}$$

The exact explicit expression for the pulling force F, which involves the integral of tractions with exponential terms (see Eq. 4), is usually not available even for the traction law given in Eq. (7). However, it is convenient to numerically calculate the pulling force for essentially arbitrary surface profile with known bond potential. Without loss in generality, we use a simplified version of the traction-separation law by approximating it to a triangle-shape profile defined by the maximum traction T_m, the separation x_m where the traction maximizes, and the failure distance c_0. So we could straightforwardly shed light on the linkage between bond properties at the atomistic level and the critical detachment at the macroscopic level. We note that T_m at x_m are directly connected with bond properties (as described in Eqs. 11 and 12) if the Bell's potential is adopted. The failure distance c_0 can also be determined by taking a point where the traction is negligible in contrast to the peak traction. For example, we may take c_0 such that traction there is one percentage of T_m. Now the simplified traction-separation law is given as

$$\frac{T(r;\delta_z)}{T_m}=\begin{cases}\frac{r-a}{x_m}, & a\le r<a+x_m\\ \frac{a+c_0-r}{c_0-x_m}, & a+x_m\le r\le a+c_0\\ 0, & \text{otherwise}\end{cases}\tag{37}$$

With the simplified version of traction in Eq. (37), we may obtain the explicit expression of force contributed by the tensile region in the contact zone

$$F_{\text{coh}}=\int_a^{a+c_0}T(r;\delta_z)2\pi r dr=\left(\int_a^{a+x_m}+\int_{a+x_m}^{a+c_0}\right)T(r;\delta_z)\,2\pi r dr\tag{38}$$

which is a function of the details of the cohesive function and the radius in contact

$$F_{\text{coh}}=\frac{\pi T_m}{3}(2ax_m+x_m^2+3ac_0+c_0^2+c_0x_m)\tag{39}$$

With Eq. (34) given by Hertz (1896), we have F_R

$$F_R=\frac{4E^*a^3}{3R}.\tag{40}$$

With Eqs. (39) and (40), we now can write the pulling force in explicit form as

$$F=F_{\text{coh}}-F_R=\frac{\pi T_m}{3}(2ax_m+x_m^2+3ac_0+c_0^2+c_0x_m)-\frac{4E^*a^3}{3R}.\tag{41}$$

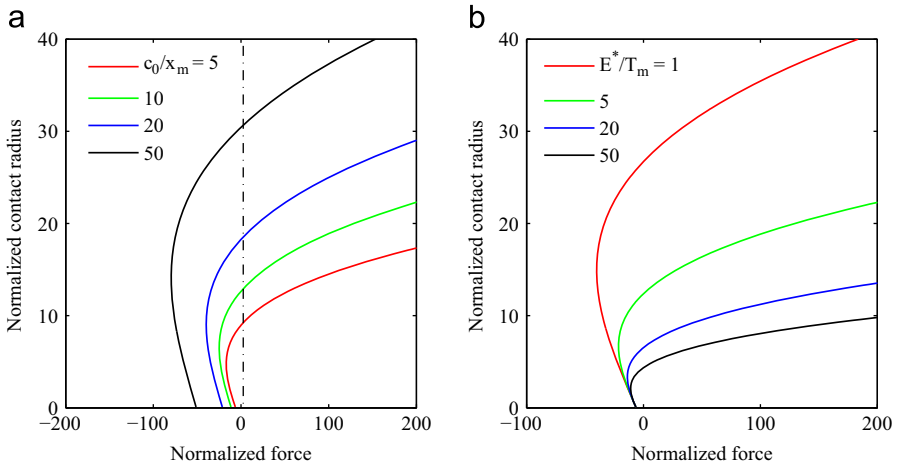

Fig. 12. Contact radius as a function of pulling force and its dependence on interfacial properties. Here the contact radius a is normalized by x_m and the pulling force is normalized by $\pi c_0 x_m T_m/3$. (a) Influence of the size of the contact zone and the location of the maximum traction at constant $E^*/T_m = 10$. (b) Influence of E^*/T_m at constant $c_0/x_m = 5$.

By applying $\partial F/\partial a = 0$, we obtain the contacting radius at which the pulling force maximizes, and this critical contacting radius is

$$a_c = \left[\frac{\pi R T_m}{12E^*}(2x_m + 3c_0)\right]^{1/2} \tag{42}$$

Eq. (42), combined with the observation in Fig. 3a, suggests why self-adhesion can be apparently higher in interfaces with long interacting distance and in compliant systems. The corresponding maximum pulling force at the critical radius $a_c$is

$$F_m = F_{\text{coh}}^{(0)} + \frac{8E^*}{3R}\left[\frac{\pi R T_m}{12E^*}(2x_m + 3c_0)\right]^{3/2}, \tag{43}$$

where $F_{\text{coh}}^{(0)}$ is the pulling force at the point $a = 0$ and is given as

$$F_{\text{coh}}^{(0)} = \frac{\pi T_m}{3}(x_m^2 + c_0^2 + c_0 x_m). \tag{44}$$

It is noted that both x_m and c_0 not only depend on the bond properties, but are also influenced by the geometrical feature of the interface (as evidently seen in Fig. 10). Once the surface profiles of the elastic media in contact are known, we can obtain the corresponding x_m and c_0. As suggested by Eqs. (42) and (33), both the contact radius at self-equilibrium and the maximum pulling-off force depend not only on the compound elastic modulus, the strength of the interface, and the spherical radius, but also on the detailed shape of the contact zone. For the contact of an sphere with an infinite half space, we show in Fig. 12 the contact radius versus pulling force curves for different interfacial properties. Fig. 12a shows how the details of the contact zone may change the adhesion and the critical pulling force; while Fig. 12b presents how the elastic properties and the strength of the interface may affect the contact radius-pulling force trajectory. Via both Eqs. (42) and (33), we demonstrate the details about how the interfacial properties may alter the contact radius-pulling force relationship, instead of using the lumped surface energy.

5. Conclusions

In this paper, we consider stochastic bonding/debonding governed adhesion in an interface composed of non-covalent bonds. When the interface is subjected to moderate stresses or deformation rate at finite temperature, we develop a stochastic model for the traction-separation response of the interface at static state and in dynamic situations. Our model is based on a simplified, and at best incomplete, model of stochastic interfaces, but it is nevertheless helpful to demonstrate the phenomenon of interest, and to predict qualitative trends. Particular examples include the evolution of pulling force during the separation of two bodies in contact via non-covalent bonds. The stress-field shown in Fig. 11 naturally describes the tensile traction at the peripheral of a contact region, and connects the influence of interfacial energy with atomistic/molecular level bonding. Its shear response, while not discussed here, could be naturally deduced if the potential energy is a function of three dimensional reaction coordinates. The dynamic response of an interface subjected to a constant pulling force resembles typical creep rupture. With growing interest in developing in-depth scientific understanding about fatigue crack growth using cohesive models (e.g., Ortiz and Pandolfi, 1999; Nguyen et al., 2001; Yang et al., 2001; Roe and Siegmund, 2003; Maiti and Geubelle, 2005; Robinson et al., 2005; Bouvard et al., 2009; Ural et al., 2009; Truong and Kitamura, 2010),

the dynamic part of the interface model presented here may help to bring in both bond dissociation and rebonding kinetics at an interface subjected to either monotonic or cyclic loading. Since the evolution of bonding probability in response to deformation plays the central role in determining the traction-separation laws of interfaces, the model naturally includes damage, strength softening, and interfacial failure in a consistent framework. It can be implemented in numerical modeling for cracking initiation and growth during fatigue fracture, and may have the potential to bring bond stochastic and bond kinetics into closer conformity with classical theories of fatigue fracture.

Acknowledgment

The research reported is supported by Chinese Academy of Sciences (KJCX2-EW-L03), MOST 973 of China (No. 2012CB937500), and National Natural Science Foundation of China (11021262).

References

Autumn, K., Sitti, M., Liang, Y.C.A., Peattie, A.M., Hansen, W.R., Sponberg, S., Kenny, T.W., Fearing, R., Israelachvili, J.N., Full, R.J., 2002. Evidence for van der Waals adhesion in gecko setae. Proc. Natl. Acad. Sci. USA 99, 12252–12256.
Barenblatt, G.I., 1959. The formation of equilibrium cracks during brittle fracture: General ideas and hypotheses, axially symmetric cracks. Appl. Math. Mech. (PMM) 23, 622–636.
Bell, G.I., 1978. Models for the specific adhesion of cells to cells. Science 200, 618–627.
Binnig, G., Quate, C.F., Gerber, C, 1986. Atomic force microscope. Phys. Rev. Lett. 56, 930–933.
Bouvard, J.L., Chaboche, J.L., Feyel, F., Gallerneau, F., 2009. A cohesive zone model for fatigue and creep-fatigue crack growth in single crystal superalloys. Int. J. Fatigue 31, 868–879.
Camacho, G.T., Ortiz, M., 1996. Computational modeling of impact damage in brittle materials. Int. J. Solids Struct. 33, 2899–2938.
Derjaguin, B.V., Muller, V.M., Toporov, Y.P., 1975. Effect of contact deformations on the adhesion of particles. J. Colloid Interface Sci. 53, 314–326.
Deshpande, V.S., McMeeking, R.M., Evans, A.G., 2006. A bio-chemo-mechanical model for cell contractility. Proc. Nat. Acad. Sci. USA 103, 14015–14020.
Deshpande, V.S., Mrksich, M., McMeeking, R.M., Evans, A.G., 2008. A bio-mechanical model for coupling cell contractility with focal adhesion formation. J. Mech. Phys. Solids 56, 1484–1510.
Dugdale, D.S., 1960. Yielding of steel sheets containing slits. J. Mech. Phys. Solids 8, 100–104.
Engler, A.J., Sen, S., Sweeney, H.L., Discher, D.E., 2006. Matrix elasticity directs stem cell lineage specification. Cell 126, 677–689.
Evans, E., Ritchie, K., 1997. Dynamic strength of molecular adhesion bonds. Biophys. J. 74, 1541–1555.
Falk, M.L., Needleman, A., Rice, J.R., 2001. A critical evaluation of cohesive zone models of dynamic fracture. In: E. van der Giessen, S. Forest, and L. Kubin (Eds.), Proceedings of the 5th European mechanics of materials conference on scale transitions from atomistics to continuum plasticity, March 5-8, 2001, Delft, the Netherlands, European Mechanics of Materials Conference, Special Issue. Journal de Physique IV, 11(Pr.5): 43–50.
Freund, L.B., 2009. Characterizing the resistance generated by a molecular bond as it is forcibly separated. Proc. Natl. Acad. Sci. USA 106, 8818–8823.
Gao, H.J., Klein, P., 1998a. Numerical simulation of crack growth in an isotropic solid with randomized internal cohesive bonds. J. Mech. Phys. Solids 46, 187–218.
Gao, Y.F., Bower, A.F., 2004. A simple technique for avoiding convergence problems in finite element simulations of crack nucleation and growth on cohesive interfaces. Modell. Simul. Mater. Sci. Eng. 12, 453–463.
Gurtin, M.E., Anand, L., 2008. Nanocrystalline grain boundaries that slip and separate: a gradient theory that accounts for grain-boundary stress and conditions at a triple-junction. J. Mech. Phys. Solids 56, 184–199.
Guduru, P.R., 2007. Detachment of a rigid solid from a wavy elastic surface - Theory. J. Mech. Phys. Solids 55, 445–472.
Hertz, H., 1896. Über die berührung fester elastischer Körper (On the contact of rigid elastic solids). In: Jones, Schott (Eds.), Journal reine und angewandte Mathematik, 92. Macmillan, London, pp. 156. (Miscellaneous Papers).
Huber, G., Gorb, S., Spolenak, R., Arzt, E., 2005. Resolving the nanoscale adhesion of individual gecko spatulae by atomic force microscopy. Biol. Lett. 1, 2–4.
Hutchinson, J.W., Evans, A.G., 2000. Mechanics of materials: top-down approaches to fracture. Acta Mater. 48, 125–135.
Jiang, L.Y., Huang, Y., Jiang, H., Ravichandran, G., Gao, H., Hwang, K.C., Liu, B., 2006. A cohesive law for carbon nanotube/polymer interfaces based on the van der Waals force. J. Mech. Phys. Solids 54, 2436–2452.
Johnson, K.L., 1985. Contact mechanics. Cambridge University Press.
Johnson, K.L., Kendall, K., Roberts, A.D., 1971. Surface energy and the contact of elastic solids. Proc. R. Soc. Lond. A 324, 301–313.
Jungbauer, S., Gao, H., Spatz, J.P., Kemkemer, R., 2008. Two characteristic regimes in frequency-dependent dynamic reorientation of fibroblasts on cyclically stretched substrates. Biophys. J. 95, 3470–3478.
Hong, S., Chew, H.B., Kim, K.S., 2009. Cohesive zone laws for void growth - I. Experimental field projection of crack-tip crazing in glassy polymers. J. Mech. Phys. Solids 57, 1357–1373.
Klein, P., Gao, H., 1998b. Crack nucleation and growth as strain localization in a virtual-bond continuum. Eng. Fract. Mech. 61, 21–48.
Koenig, S.P., Boddeti, N.G., Dunn, M.L., Bunch, J.S., 2011. Ultrastrong adhesion of graphene membranes. Nat. Nanotechnol. 6, 543–546.
Kramers, H.A., 1940. Brownian motion in a field of force and the diffusion model of chemical reactions. Physica 7, 284–304.
Lin, Y., Freund, L.B., 2007. An lower bound on receptor density for stable cell adhesion due to thermal undulations. J. Mater. Sci. 42, 8904–8910.
Lin, Y., Inamdar, M., Freund, L.B., 2008. The competition between Brownian motion and adhesion in soft materials. J. Mech. Phys. Solids 56, 241–250.
Lo, C.M., Wang, H.B., Dembo, M., Wang, Y.L., 2000. Cell movement is guided by the rigidity of the substrate. Biophys. J. 79, 144–152.
Maiti, S., Geubelle, P.H., 2005. A cohesive model for fatigue failure of polymers. Eng. Fract. Mech. 72, 691–708.
Marshall, B.T., Long, M., Piper, J.W., Yago, T., McEver, R.P., Zhu, C., 2003. Direct observation of catch bonds involving cell-adhesion molecules. Nature 423, 190–193.
Needleman, A., 1990. An analysis of decohesion along an imperfect interface. Int. J. Fract. 42, 21–40.
Nguyen, O., Repetto, E.A., Ortiz, M., Radovitzky, R.A., 2001. A cohesive model of fatigue crack growth. Int. J. Fract. 110, 351–369.
Ortiz, M., Pandolfi, A., 1999. Finite-deformation irreversible cohesive elements for three-dimensional crack-propagation analysis. Int. J. Numer. Methods Eng. 44, 1267–1282.
Phan, U.T., Waldron, T.T., Springer, T.A., 2006. Remodeling of the lectin-EGF-like domain interface in P- and L-selectin increases adhesiveness and shear resistance under hydrodynamic force. Nat. Immunol. 7, 883–889.
Qian, J., Wang, J., Gao, H., 2008. Lifetime and strength of adhesive molecular bond clusters between elastic media. Langmuir 24, 1262–1270.
Qian, J., Wang, J., Yuan, L., Gao, H.J., 2009. Lifetime and strength of periodic bond clusters between elastic media under inclined loading. Biophys. J. 97, 2438–2445.
Robinson, P., Galvanetto, U., Tumino, D., Bellucci, G., Violeau, D., 2005. Numerical simulation of fatigue-driven delamination using interface elements. Int. J. Numer. Methods Eng. 63, 1824–1848.
Roe, K.L., Siegmund, T., 2003. An irreversible cohesive zone model for interface fatigue crack growth simulation. Eng. Fract. Mech. 70, 209–232.

Smith, B.L., Schäffer, T.E., Viani, M., Thompson, J.B., Frederick, N.A., Kindt, J., Belcher, A., Stucky, G.D., Morse, D.E., Hansma, P.K., 1999. Molecular mechanistic origin of the toughness of natural adhesives, fibres and composites. Nature 399, 761–763.
Su, C., Wei, Y.J., Anand, L., 2004. An elastic-plastic interface constitutive model: application to adhesive joints. Int. J. Plasticity 20, 2063–2081.
Thomas, W.E., Trintchina, E., Forero, M., Vogel, V., Sokurenko, E.V., 2002. Bacterial adhesion to target cells enhanced by shear force. Cell 109, 913–923.
Tidball, J.G., 2005. Mechanical signal transduction in skeletal muscle growth and adaptation. J. Appl. Physiol. 98, 1900–1908.
Truong, D.V., Kitamura, T., 2010. Cohesive zone model applied to creep crack initiation at an interface edge between submicron thick films. Int. J. Damage Mech. 19, 301–319.
Tvergaard, V., Hutchinson, J.W., 1992. The relation between crack growth resistance and fracture process parameters in elastic-plastic solids. J. Mech. Phys. Solids 40, 1377–1397.
Ural, A., Krishnan, V.R., Papoulia, K.D., 2009. A cohesive zone model for fatigue crack growth allowing for crack retardation. Int. J. Solids Struct. 46, 2453–2462.
Wang, J.Z., Gao, H.J., 2008. Clustering instability in adhesive contact between elastic solids via diffusive molecular bonds. J. Mech. Phys. Solids 56, 251–266.
Warner, D.H., Sansoz, F., Molinari, J.F., 2006. Atomistic-based continuum investigation of plastic deformation in nanocrystalline copper. Int. J. Plasticity 22, 754–774.
Wei, Y.J., Anand, L., 2004. Grain-boundary sliding and separation in polycrystalline metals: application to nanocrystalline f.c.c. metals. J. Mech. Phys. Solids 52, 2587–2616.
Wei, Y.J., 2008a. Physical interpretation of the maximum receptor-ligand bond spacing to ensure cell adhesion in ligand-coated substrates. Langmuir 24, 5644–5646.
Wei, Y.J., 2008b. Entropic-elasticity-controlled dissociation and energetic-elasticity-controlled rupture induce catch-to-slip bonds in cell-adhesion molecules. Phys. Rev. E 77, 031910.
Wei, Y.J., Gao, H., Bower, A.F., 2009. Numerical simulations of crack deflection at a twist misoriented grain boundary between two ideally brittle crystals. J. Mech. Phys. Solids 57, 1865–1879.
Wei, Y.J., Bower, A.F., Gao, H., 2010. Analytical model and molecular dynamics simulations of the size dependence of flow stress in amorphous intermetallic nanowires at temperatures near the glass transition. Phys. Rev. B 81, 125402.
Weisstein, E.W. 2014. Fermi-Dirac Distribution. ⟨http://mathworld.wolfram.com/Fermi-DiracDistribution.html⟩.
Wei, Y.G., Hutchinson, J.W., 1997. Nonlinear delamination mechanics for thin films. J. Mech. Phys. Solids 45, 1137–1159.
Wiita, A.P., Perez-Jimenez, R., Walther, K.A., Gräter, F., Berne, B.J., Holmgren, A., Sanchez-Ruiz, J.M., Fernandez, J.M., 2007. Probing the chemistry of thioredoxin catalysis with force. Nature 450, 124–127.
Xu, X.P., Needleman, A., 1994. Numerical simulations of fast crack growth in brittle solids. J. Mech. Phys. Solids 42, 1397–1434.
Yang, B., Mall, S., Ravi-Chandar, K.A., 2001. A cohesive zone model for fatigue crack growth in quasibrittle materials. Int. J. Solids Struct. 38, 3927–3944.
Yang, Q.D., Thouless, M.D., Ward, S.M., 1999. Numerical simulations of adhesively-bonded beams failing with extensive plastic deformation. J. Mech. Phys. Solids 47, 1337–1353.
Zacharia, R., Ulbricht, H., Hertel, T., 2004. Interlayer cohesive energy of graphite from thermal desorption of polyaromatic hydrocarbons. Phys. Rev. B 69, 155406.
Zhurkov, S.N., 1965. Kinetic concept of the strength of solids. Int. J. Fract. Mech. 1, 311–322.